

## Article

# Luminescence and Scintillation in the Niobium Doped Oxyfluoride $\text{Rb}_4\text{Ge}_5\text{O}_9\text{F}_6:\text{Nb}$

Darren Carone <sup>1</sup>, Vladislav V. Klepov <sup>1</sup>, Scott T. Misture <sup>2</sup>, Joseph C. Schaeperkoetter <sup>2</sup>, Luiz G. Jacobsohn <sup>3</sup>, Mina Aziziha <sup>4</sup>, Juliano Schorne-Pinto <sup>4</sup>, Stuart A. J. Thomson <sup>5</sup>, Adrian T. Hines <sup>1</sup>, Theodore M. Besmann <sup>4</sup>, and Hans-Conrad zur Loye <sup>1,\*</sup>

- <sup>1</sup> Department of Chemistry and Biochemistry, University of South Carolina, Columbia, SC 29208, USA; dcarone@email.sc.edu (D.C.); klepov@northwestern.edu (V.V.K.); hinesat@email.sc.edu (A.T.H.)
- <sup>2</sup> Kazuo Inamori School of Engineering, Alfred University, Alfred, NY 14802, USA; misture@alfred.edu (S.T.M.); schaeperkoetter@alfred.edu (J.C.S.)
- <sup>3</sup> Department of Materials Science and Engineering, Clemson University, Clemson, SC 29634, USA; luiz@g.clemson.edu
- <sup>4</sup> Nuclear Engineering Program, Department of Mechanical Engineering, University of South Carolina, Columbia, SC 29208, USA; maziziha@mailbox.sc.edu (M.A.); julianos@mailbox.sc.edu (J.S.-P.); besmann@sc.edu (T.M.B.)
- <sup>5</sup> Edinburgh Instruments Ltd., 2 Bain Square, Livingston EH54 7DQ, UK; stuart.thomson@edinst.com
- \* Correspondence: zurloye@mailbox.sc.edu



**Citation:** Carone, D.; Klepov, V.V.; Misture, S.T.; Schaeperkoetter, J.C.; Jacobsohn, L.G.; Aziziha, M.; Schorne-Pinto, J.; Thomson, S.A.J.; Hines, A.T.; Besmann, T.M.; et al. Luminescence and Scintillation in the Niobium Doped Oxyfluoride  $\text{Rb}_4\text{Ge}_5\text{O}_9\text{F}_6:\text{Nb}$ . *Inorganics* **2022**, *10*, 83. <https://doi.org/10.3390/inorganics10060083>

Academic Editors: Duncan H. Gregory, Torben R. Jensen, Claudio Pettinari, Vladimir Arion, Wolfgang Linert and Richard Dronskowski

Received: 27 May 2022

Accepted: 14 June 2022

Published: 16 June 2022

**Publisher's Note:** MDPI stays neutral with regard to jurisdictional claims in published maps and institutional affiliations.



**Copyright:** © 2022 by the authors. Licensee MDPI, Basel, Switzerland. This article is an open access article distributed under the terms and conditions of the Creative Commons Attribution (CC BY) license (<https://creativecommons.org/licenses/by/4.0/>).

**Abstract:** A new niobium-doped inorganic scintillating oxyfluoride,  $\text{Rb}_4\text{Ge}_5\text{O}_9\text{F}_6:\text{Nb}$ , was synthesized in single crystal form by high-temperature flux growth. The host structure,  $\text{Rb}_4\text{Ge}_5\text{O}_9\text{F}_6$ , crystallizes in the orthorhombic space group *Pbcn* with lattice parameters  $a = 6.98430(10)$  Å,  $b = 11.7265(2)$  Å, and  $c = 19.2732(3)$  Å, consisting of germanium oxyfluoride layers made up of  $\text{Ge}_3\text{O}_9$  units connected by  $\text{GeO}_3\text{F}_3$  octahedra. In its pure form,  $\text{Rb}_4\text{Ge}_5\text{O}_9\text{F}_6$  shows neither luminescence nor scintillation but when doped with niobium,  $\text{Rb}_4\text{Ge}_5\text{O}_9\text{F}_6:\text{Nb}$  exhibits bright blue luminescence and scintillation. The isostructural doped structure,  $\text{Rb}_4\text{Ge}_5\text{O}_9\text{F}_6:\text{Nb}$ , crystallizes in the orthorhombic space group *Pbcn* with lattice parameters  $a = 6.9960(3)$  Å,  $b = 11.7464(6)$  Å, and  $c = 19.3341(9)$  Å. X-ray absorption near edge structure (XANES) and extended X-ray absorption fine structure (EXAFS) measurements suggest that the niobium is located in an octahedral coordination environment. Optical measurements inform us that the niobium dopant acts as the activator. The synthesis, structure, and optical properties are reported, including radioluminescence (RL) measurements under X-ray irradiation.

**Keywords:** flux crystal growth; crystal structure; photoluminescence; scintillation

## 1. Introduction

A commonly observed process in inorganic materials is luminescence, where UV light-excited electrons return to the ground state via the emission of light. Less common is the additional ability of some of these materials to scintillate, where X-ray,  $\gamma$ -ray, or energetic particles are the source of excitation. These materials find use as X-ray phosphors and scintillators for positron emission tomography (PET) [1], computer tomography (CT) scanners [2], and more recently, by homeland security for improved nuclear detection systems.

Traditional approaches for the discovery of new luminescent (and potentially scintillating) inorganic materials include trial-and-error incorporation of chemical elements such as  $\text{Ce}^{3+}$  into the crystal structure. These elements can either fully occupy a crystallographic site, thus creating an intrinsic scintillator, or can change a small percentage of the host composition thus creating an extrinsic scintillator. In the latter case, often the location of the dopant in the crystal structure cannot be determined with certainty.

It is known that several  $d^0$  cations, such as  $\text{Nb}^{5+}$ ,  $\text{Ta}^{5+}$ , or  $\text{W}^{6+}$ , can exhibit intense luminescence and scintillation as self-activated luminescent oxides, with  $\text{MgWO}_4$  being

a well-known example [3]. Our research group has explored the synthesis of new oxide and oxyfluoride materials via several different synthetic routes, resulting in the discovery of new luminescent and scintillating materials. This has recently led to the discovery of a new self-activated luminescent silicate  $\text{Rb}_4\text{Ta}_2\text{Si}_8\text{O}_{23}$  that exhibits bright blue scintillation when exposed to X-rays [4]. These efforts were continued, targeting oxyfluoride type materials that are less abundant in the literature likely due to the relative ease with which oxides containing inherently luminescent ions can be prepared using traditional solid-state syntheses or hydrothermal methods. In contrast, creating oxyfluoride environments for luminescent ions is much more challenging, as it requires a delicate balance between oxygen and fluorine content. For this reason, we pursued flux crystal growth using metal fluoride reagents in air to encourage the formation of oxyfluorides. Using such approaches, our group has explored the synthesis of new oxide and oxyfluoride materials via several different synthetic routes aimed at the discovery of new luminescent and scintillating materials [5–11]. This resulted in luminescing and scintillating flux-grown crystals of lanthanide-containing silicates  $\text{Cs}_3\text{RESi}_4\text{O}_{10}\text{F}$  (RE = Eu and Tb) [12], whose optical properties support the proposed idea that the incorporation of fluorine into the crystal structure can lead to increased fluorescence intensity. In addition, it led to a new hydrothermally synthesized tungsten-based oxyfluoride,  $\text{BaWO}_2\text{F}_4$ , exhibiting intense, intrinsic, X-ray scintillation, where the isolated  $\text{WO}_2\text{F}_4^{2-}$  species functions as the luminescence and scintillation center [13].

These discoveries prompted us to perform additional syntheses of new oxyhalide, especially oxyfluoride, materials, and to target the incorporation of inherently optically inactive cations,  $\text{Nb}^{5+}$ ,  $\text{Ta}^{5+}$ , or  $\text{W}^{6+}$ , which are, however, known to luminesce when located in a mixed oxide fluoride coordination environment [14–16]. Herein, we report the synthesis, crystal structure, and optical properties of a new host material,  $\text{Rb}_4\text{Ge}_5\text{O}_9\text{F}_6$ , which, when doped with the inherently optically inactive  $\text{Nb}^{5+}$  through high-temperature flux growth to form  $\text{Rb}_4\text{Ge}_5\text{O}_9\text{F}_6:\text{Nb}$ , luminesces in a bright blue color under UV-light excitation, and also scintillates under X-ray exposure. The photoluminescence quantum yield is reported, and the scintillation response was studied by radioluminescence (RL) measurements. The local coordination of the Nb dopant was investigated by extended X-ray absorption fine structure (EXAFS).

## 2. Experimental Section

### 2.1. Reagents

$\text{RbCl}$  (BeanTown Chemical, Hudson, NH, USA, 99%),  $\text{GeO}_2$  (Alfa Aesar, Tewksbury, MA, USA, 99.999%), and  $\text{Nb}_2\text{O}_5$  (Alfa Aesar, 99.9%) were used as received.  $\text{RbF}$  (Strem, Newburyport, MA, USA, 99.8%) was also used as received, although found to be  $\text{HRbF}_2$  following powder X-ray diffraction analysis.

### 2.2. Crystal Growth

Single crystals of  $\text{Rb}_4\text{Ge}_5\text{O}_9\text{F}_6$  were grown by layering a mixture of 2 mmol  $\text{GeO}_2$  beneath a mixture of 14 mmol of  $\text{RbCl}$  and 12.5 mmol of  $\text{RbF}$ . Reagents were added to a cylindrical silver crucible (1.2 cm D  $\times$  5.7 cm H) that was heated to 900 °C in air, held at that temperature for 12 h, slowly cooled to 450 °C at a rate of 6 °C/h, and finally cooled to room temperature by turning off the furnace. The solidified flux matrix was dissolved in water aided by sonication, and the products were isolated via vacuum filtration. Thin, colorless plate crystals were produced along with large amounts of  $\text{AgCl}$  powder, which was removed using a concentrated solution of sodium thiosulfate. Crystals of  $\text{Rb}_4\text{Ge}_5\text{O}_9\text{F}_6$  grown in these reactions do not exhibit any luminescence properties under UV exposure.

Performing the same crystal growth procedure, but adding  $\text{Nb}_2\text{O}_5$  as a dopant by layering a mixture of 2 mmol  $\text{GeO}_2$  and 0.5 mmol  $\text{Nb}_2\text{O}_5$  beneath a mixture of 14 mmol of  $\text{RbCl}$  and 12.5 mmol of  $\text{RbF}$ , resulted in single crystals of  $\text{Rb}_4\text{Ge}_5\text{O}_9\text{F}_6:\text{Nb}$ . Again, thin, colorless plate crystals (Figure 1) were produced along with  $\text{AgCl}$ , which was removed from the crystals using sodium thiosulfate. This time, however, the crystals exhibited significant luminescence under UV exposure.

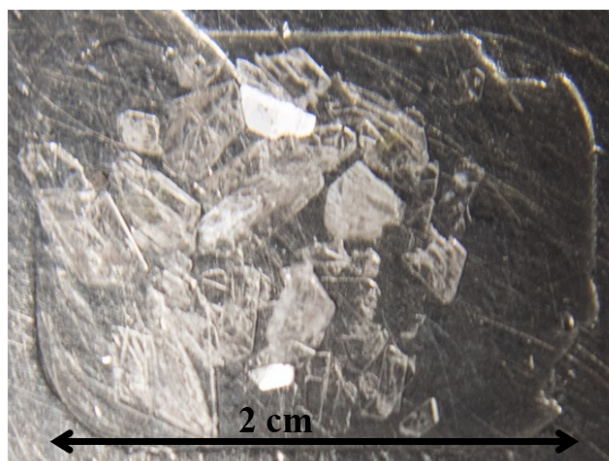


**Figure 1.** Optical microscopy image showing representative crystals of  $\text{Rb}_4\text{Ge}_5\text{O}_9\text{F}_6:\text{Nb}$ .

### 2.3. Single-Crystal X-ray Diffraction

Single-crystal X-ray diffraction data were collected on crystals produced from reactions with and without  $\text{Nb}_2\text{O}_5$ , at 300(2) K on a Bruker (Madison, WI, USA) D8 QUEST diffractometer equipped with an Incoatec (Geesthacht, Germany)  $\text{I}\mu\text{S}$  3.0 microfocus radiation source ( $\text{MoK}\alpha$ ,  $\lambda = 0.71073 \text{ \AA}$ ) and a PHOTON II area detector. The crystals were mounted on a microloop using immersion oil. The raw data reduction and absorption corrections were performed using SAINT+ and SADABS programs [17,18]. Initial structure solutions were obtained with SHELXS-2017 using direct methods and Olex2 GUI [19]. Full-matrix least-square refinements against  $F^2$  were performed with SHELXL software (Version 2018/3, Georg-August Universität Göttingen, Göttingen, Germany) [20]. The structures were checked for missing symmetry with the Addsym program implemented within PLATON software (Version 200322, Utrecht University, Utrecht, The Netherlands), and no higher symmetry was found [21].

Initial refinement of the structure of the undoped crystal with all anion sites modeled as oxygens resulted in an R1 value of 2.20%, with the highest residual electron density peaks (max peak =  $1.23 \text{ e}^- / \text{\AA}^3$ ) being adjacent to three of the anion sites, and a formula of  $\text{Rb}_4\text{Ge}_5\text{O}_{15}$ , which has an excess charge of  $-6$ . The excess negative charge and the residual electron density peaks adjacent to the anion sites were both clear indicators that the material was an oxyfluoride. Freely refining the occupancy of all the oxygen sites resulted in five oxygen sites with occupancies close to unity (103–104%) and three oxygen sites, those with the high adjacent residual electron density peaks, with much higher occupancies (124–126%). Freely refining these latter three sites as fluorine sites resulted in occupancies near unity (102–103%). Fixing all anion site occupancies to unity then resulted in the charge balanced formula of  $\text{Rb}_4\text{Ge}_5\text{O}_9\text{F}_6$ , the highest residual electron density peaks (max peak =  $0.728 \text{ e}^- / \text{\AA}^3$ ) being located among the Rb atoms between the slabs, and a final R1 value of 1.52%. The crystallographic data and results of the diffraction experiments for  $\text{Rb}_4\text{Ge}_5\text{O}_9\text{F}_6$  and  $\text{Rb}_4\text{Ge}_5\text{O}_9\text{F}_6:\text{Nb}$  are summarized in Table 1. No differences in the structural models for  $\text{Rb}_4\text{Ge}_5\text{O}_9\text{F}_6$  and  $\text{Rb}_4\text{Ge}_5\text{O}_9\text{F}_6:\text{Nb}$  were observed, and no additional electron density was located that could indicate the location of the Nb in the  $\text{Rb}_4\text{Ge}_5\text{O}_9\text{F}_6:\text{Nb}$  structure. Select bond lengths for  $\text{Rb}_4\text{Ge}_5\text{O}_9\text{F}_6$  and  $\text{Rb}_4\text{Ge}_5\text{O}_9\text{F}_6:\text{Nb}$  are listed in Table 2.

**Table 1.** Crystallographic data for  $\text{Rb}_4\text{Ge}_5\text{O}_9\text{F}_6$  and  $\text{Rb}_4\text{Ge}_5\text{O}_9\text{F}_6:\text{Nb}$ .

Empirical Formula	$\text{Rb}_4\text{Ge}_5\text{O}_9\text{F}_6$	$\text{Rb}_4\text{Ge}_5\text{O}_9\text{F}_6:\text{Nb}$
Temperature (K)	302(2)	303(2)
Wavelength (Å)	0.71073	0.71073
Space group, Z	<i>Pbcn</i> , 4	<i>Pbcn</i> , 4
Unit cell dimensions (Å)	<i>a</i> = 6.98430(10) <i>b</i> = 11.7265(2) <i>c</i> = 19.2732(3)	<i>a</i> = 6.9960(3) <i>b</i> = 11.7464(6) <i>c</i> = 19.3341(9)
Volume (Å <sup>3</sup> )	1578.50(4)	1588.83(13)
Density (calculated) (g/cm <sup>3</sup> )	4.051	4.025
Absorption coefficient (mm <sup>-1</sup> )	21.768	21.626
<i>F</i> (000)	1736	1736
Crystal size (mm × mm × mm)	0.06 × 0.03 × 0.02	0.04 × 0.03 × 0.005
Theta range for data collection (°)	3.40 to 36.31	3.39 to 31.61
Index ranges	$-9 \leq h \leq 9, -16 \leq k \leq 16,$ $-27 \leq l \leq 24$	$-9 \leq h \leq 9, -16 \leq k \leq 16,$ $-27 \leq l \leq 27$
Reflections collected	36,504	106,148
Independent reflections	2297 [ <i>R</i> <sub>(int)</sub> = 0.0410]	2317 [ <i>R</i> <sub>(int)</sub> = 0.0890]
Data/restraints/parameters	2297/0/120	2317/0/119
Goodness-of-fit on <i>F</i> <sup>2</sup>	1.144	1.089
Final <i>R</i> indices [ <i>I</i> > 2σ( <i>I</i> )]	<i>R</i> <sub>1</sub> = 0.0152, <i>wR</i> <sub>2</sub> = 0.0335	<i>R</i> <sub>1</sub> = 0.0245, <i>wR</i> <sub>2</sub> = 0.0513
<i>R</i> indices (all data)	<i>R</i> <sub>1</sub> = 0.0164, <i>wR</i> <sub>2</sub> = 0.0338	<i>R</i> <sub>1</sub> = 0.0335, <i>wR</i> <sub>2</sub> = 0.0563
Largest diff. peak and hole	0.728 and $-0.464 \text{ e}^- / \text{Å}^3$	1.464 and $-0.873 \text{ e}^- / \text{Å}^3$

**Table 2.** Selected interatomic distances (Å) for  $\text{Rb}_4\text{Ge}_5\text{O}_9\text{F}_6$  and  $\text{Rb}_4\text{Ge}_5\text{O}_9\text{F}_6:\text{Nb}$ .

Interaction	$\text{Rb}_4\text{Ge}_5\text{O}_9\text{F}_6$	$\text{Rb}_4\text{Ge}_5\text{O}_9\text{F}_6:\text{Nb}$
Ge1-F1	1.8290(12)	1.828(2)
Ge1-F2	1.8252(12)	1.831(2)
Ge1-F3	1.8374(12)	1.841(2)
Ge1-O1	1.8237(14)	1.833(3)
Ge1-O2	1.8569(14)	1.863(3)
Ge1-O5	1.8527(14)	1.861(3)
Ge2-O1	1.7168(14)	1.714(3)
Ge2-O2	1.7607(10)	1.727(3)
Ge2-O3	1.7232(14)	1.7614(18)
Ge2-O4	1.7777(13)	1.779(3)
Ge3-O4	1.7727(13)	1.772(3)
Ge3-O4	1.7727(13)	1.772(3)
Ge3-O5	1.7269(14)	1.728(3)
Ge3-O5	1.7270(14)	1.728(3)

#### 2.4. Powder X-ray Diffraction (PXRD)

Powder X-ray diffraction data were collected on a Bruker D2 Phaser powder X-ray diffractometer using Cu K $\alpha$  radiation. The step scan covered the angular range 5–65° 2 $\theta$  in steps of 0.04°. Experimental and calculated PXRD data for Rb<sub>4</sub>Ge<sub>5</sub>O<sub>9</sub>F<sub>6</sub>:Nb are provided in Figure S1.

#### 2.5. Inductively Coupled Plasma Optical Emission Spectrometry (ICP-OES)

ICP-OES was performed using a Perkin Elmer (Waltham, MA, USA) Avio 200 spectrometer on digested samples of Rb<sub>4</sub>Ge<sub>5</sub>O<sub>9</sub>F<sub>6</sub> and Rb<sub>4</sub>Ge<sub>5</sub>O<sub>9</sub>F<sub>6</sub>:Nb. The digestion process was carried out with a PerkinElmer's Titan MPS microwave sample preparation system. Crystalline samples of around 10.0 mg were loaded in Teflon™ vials with 8 mL of aqua regia (ratio mixture of 8 mL HNO<sub>3</sub>, 4 mL of HCl, and 3 mL of DI water). The Teflon™ vials were placed in a microwave-programmable oven. The temperature increased to 175 °C by 5 °C/min and 30 bars. Then, the samples were held at this temperature for 10 min followed by cooling to 50 °C at 1 °C/min. The samples were then cooled down to room temperature without rate control for two hours before removing the vials. The dissolved samples in aqua regia solutions were diluted to achieve the appropriate concentrations using 5 wt% HNO<sub>3</sub> in water. The calibration curves were measured for Rb, Ge, and Nb in various concentrations and using appropriate optical mode (by radial or axial detectors). The molar ratio of the mixed salts was determined by ICP-OES for digested samples calibrated by the High-Purity Standards (HPS). The overall precision was  $\pm 1$  mole%.

#### 2.6. Optical Properties

The photoluminescence response was determined using an Edinburgh Instruments (Livingston, United Kingdom) FLS1000 photoluminescence spectrometer on ground single crystals of Rb<sub>4</sub>Ge<sub>5</sub>O<sub>9</sub>F<sub>6</sub>:Nb. The emission scan was collected at an excitation wavelength of 254 nm. The photoluminescence quantum yield was measured using an Edinburgh Instruments FS5 Spectrofluorometer with an SC-30 integrating sphere.

#### 2.7. Scintillation

Radioluminescence (RL) measurements were carried out using a customer-designed configuration of the Freiberg Instruments (Freiberg, Germany) Lexsyg spectrofluorometer equipped with a Varian Medical Systems (Crawley, United Kingdom) VF-50J X-ray tube with a tungsten target. The X-ray source was coupled with a Crystal Photonics CXD-S10 photodiode for continuous radiation intensity monitoring. The light emitted by the sample was collected by an Andor Technology (Belfast, United Kingdom) SR-OPT-8024 optical fiber connected to an Andor Technology Shamrock 163 spectrograph coupled to a cooled (−80 °C) Andor Technology DU920P-BU Newton CCD camera (spectral resolution of ~0.5 nm/pixel). Powdered sample was filled into ~8 mm diameter, 0.5 mm deep cups, thus allowing for relative RL intensity between different samples. Bismuth germanium oxide (BGO) powder (Alfa Aesar Puratronic, 99.9995% (metals basis)) was used as a reference. RL was measured under continuous X-ray irradiation (W lines together with bremsstrahlung radiation) 40 kV, 1 mA) with an integration time of 5 s. RL measurements as a function of temperature were executed under continuous heating with a 0.5 °C/s heating rate up to 450 °C and a 10 s integration time. Thus, temperature increased by 5 °C during the acquisition of each spectrum. Spectra were labeled by the starting acquisition temperature. Spectra were automatically corrected using the spectral response of the system determined by the manufacturer.

Scintillation images of Rb<sub>4</sub>Ge<sub>5</sub>O<sub>9</sub>F<sub>6</sub>:Nb single crystals were taken using a digital camera inside a Rigaku (Tokyo, Japan) Ultima IV diffractometer equipped with a Cu K $\alpha$  source ( $\lambda = 1.54018$  Å).

## 2.8. Extended X-ray Absorption Fine Structure (EXAFS)

Specimens for EXAFS analysis were prepared for a known crystalline sample,  $\text{Cs}_5\text{Nb}_3\text{O}_3\text{F}_{14}$ , and for Nb-doped  $\text{Rb}_4\text{Ge}_5\text{O}_9\text{F}_6$ , by dilution of the sample with BN to achieve approximately 1 absorption length attenuation in transmission geometry at the Nb K edge. Samples were measured at the MRCAT beamline (10-ID) at the Advanced Photon Source. Both transmission and fluorescence signals were collected in parallel for both specimens and the fluorescence data were corrected for self-absorption. Data analysis was performed using the Demeter suite [22].

## 3. Results and Discussion

### 3.1. Crystal Structure

The host structure,  $\text{Rb}_4\text{Ge}_5\text{O}_9\text{F}_6$ , crystallizes in the orthorhombic space group  $Pbcn$  with lattice parameters of  $a = 6.98430(10)$  Å,  $b = 11.7265(2)$  Å, and  $c = 19.2732(3)$  Å. The crystal structure is composed of germanium oxyfluoride layers consisting of isolated  $\text{GeO}_3\text{F}_3$  octahedra that are connected by cyclic  $\text{Ge}_3\text{O}_9$  units (Figure 2c); the cyclic  $\text{Ge}_3\text{O}_9$  units were previously observed in the optically inactive  $(\text{NH}_4)_4[(\text{GeO}_2)_3(\text{GeO}_{1.5}\text{F}_3)_2] \cdot 0.67\text{H}_2\text{O}$  [23]. The  $\text{GeO}_3\text{F}_3$  octahedra in  $\text{Rb}_4\text{Ge}_5\text{O}_9\text{F}_6$ , shown in Figure 2a, have three Ge-O bonds with distances of 1.821(2)–1.859(2) Å, and three, on average, slightly shorter Ge-F bonds with distances of 1.825(2)–1.8371(19) Å. Cyclic  $\text{Ge}_3\text{O}_9$  units, shown in Figure 2b, consisting of corner sharing  $\text{GeO}_4$  tetrahedra with Ge-O bond lengths of 1.717(2)–1.7791(19) Å, connect the  $\text{GeO}_3\text{F}_3$  octahedra through each oxygen atom to form the  $\text{Ge}_5\text{O}_9\text{F}_6^{4-}$  germanium oxyfluoride layers. The fluorine atoms terminate the layers and are oriented towards the Rb atoms, which separate the layers. The layers repeat along the c-axis to form the overall structure, shown in Figure 3.

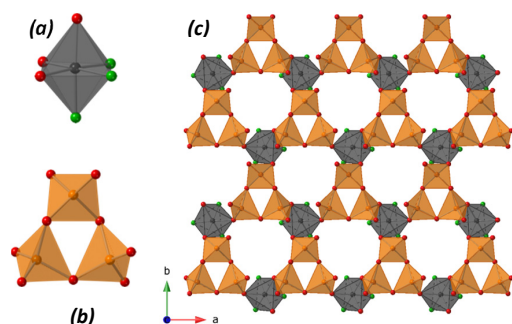


**Figure 2.** Illustration of (a)  $\text{GeO}_3\text{F}_3$  octahedra, (b)  $\text{Ge}_3\text{O}_9$  unit, and (c) their connectivity to form the germanium oxyfluoride layer. Germanium octahedra are shown in grey, germanium tetrahedra in orange, oxygen in red, and fluorine in green.

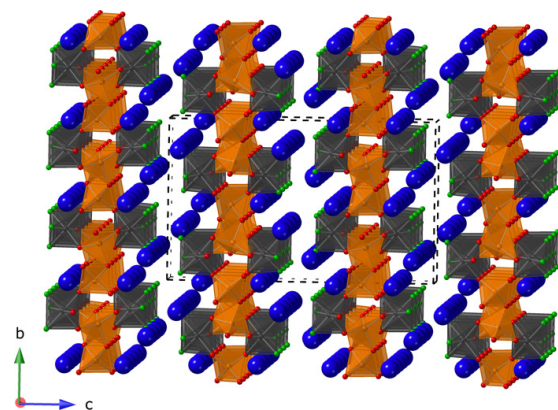


**Figure 3.** Representation of the single crystal structure of  $\text{Rb}_4\text{Ge}_5\text{O}_9\text{F}_6$ . Rubidium atoms are shown in blue,  $\text{GeO}_3\text{F}_3$  octahedra in grey,  $\text{GeO}_4$  tetrahedra in orange, oxygen atoms in red, and fluorine atoms in green.

### 3.2. Optical Properties

Crystals of  $\text{Rb}_4\text{Ge}_5\text{O}_9\text{F}_6:\text{Nb}$  were found to exhibit room-temperature luminescence when exposed to UV light. The emission spectrum for  $\text{Rb}_4\text{Ge}_5\text{O}_9\text{F}_6:\text{Nb}$ , when excited at 254 nm, is shown in Figure 4. It can be seen that the material exhibits fluorescence with one broad emission peak in the 375–650 nm range. The broad peak is centered at  $\sim 478$  nm, which lies within the blue region of the visible spectrum and is consistent with the blue emission observed in crystals exposed to 254 nm UV light, shown in the Figure 4 inset. The photoluminescence quantum yield was measured on a powder sample and was found to be 17.9%. Due to the lack of a luminescent center and the absence of luminescence in the pure  $\text{Rb}_4\text{Ge}_5\text{O}_9\text{F}_6$  host crystals, but the presence of luminescence in  $\text{Rb}_4\text{Ge}_5\text{O}_9\text{F}_6:\text{Nb}$ , we conclude that Nb doping is responsible for the observed luminescence. To confirm and quantify the presence of Nb in  $\text{Rb}_4\text{Ge}_5\text{O}_9\text{F}_6$ , the elemental composition of the crystals was measured using ICP-OES. Several single crystals grown from reactions containing  $\text{Nb}_2\text{O}_5$  were digested in aqua regia and analyzed for Rb, Ge, and Nb concentrations. For comparison and as a control, single crystals grown in the absence of the  $\text{Nb}_2\text{O}_5$  precursor, which exhibit no room temperature luminescence, were also digested in aqua regia and the same analysis was performed. It was determined that the crystals grown in the presence of  $\text{Nb}_2\text{O}_5$  contained an average concentration of 0.82(6)% atomic percent Nb (cationic), while the sample grown in the absence of Nb yielded a measured concentration of  $<0.01\%$  atomic percent, which is within the experimental uncertainty of the technique. The experimental results clearly indicate the presence of Nb within the crystals and corroborate the importance of Nb for the luminescence activation of  $\text{Rb}_4\text{Ge}_5\text{O}_9\text{F}_6$ .

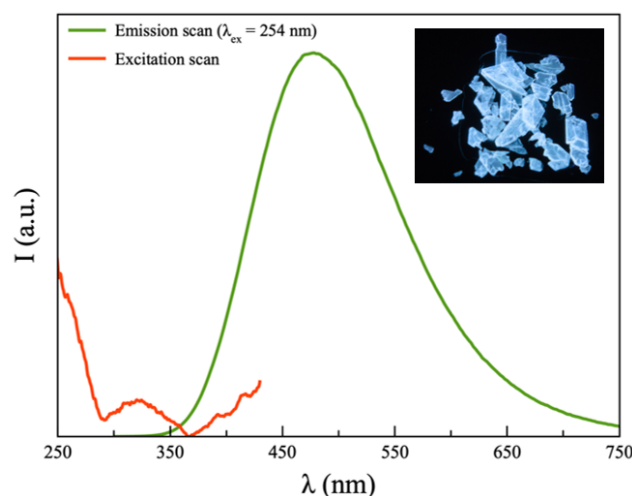


**Figure 4.** Photoluminescence spectra and optical image of  $\text{Rb}_4\text{Ge}_5\text{O}_9\text{F}_6:\text{Nb}$  crystals under UV light.

Crystals of  $\text{Rb}_4\text{Ge}_5\text{O}_9\text{F}_6:\text{Nb}$  were also found to scintillate upon exposure to X-rays ( $\text{Cu K}\alpha$  radiation) and the blue scintillation is shown in Figure 5. The scintillation response of powdered  $\text{Rb}_4\text{Ge}_5\text{O}_9\text{F}_6:\text{Nb}$  was investigated under X-ray irradiation through RL measurements. Figure 6 shows the RL spectrum for  $\text{Rb}_4\text{Ge}_5\text{O}_9\text{F}_6:\text{Nb}$ , with the most intense spectrum acquired just above room temperature. The similarities of this spectrum to the emission spectrum under 254 nm light are clear, with the maximum of the RL spectrum occurring at 480 nm. Integral emission was determined to be  $\sim 2\%$  of BGO powder at room temperature.

The scintillation thermal quenching was investigated through the acquisition of RL spectra at high temperatures (Figure 6) [24–27]. As expected, the peak intensity was quenched with increasing temperature, and no emissions were observed above about 400 °C. Figure 7 highlights the behavior of peak intensity as a function of temperature. A short plateau up to about 350 K followed by a continuous decay was fitted using the Mott-Seitz model, where the RL intensity  $I$  is given by:  $I = I_0 / (1 + Ce^{-W/kT})$ , with  $I_0$  being

the intensity at room temperature,  $W$  the activation energy for non-radiative recombination,  $k$  Boltzman's constant,  $T$  the temperature in K, and  $C$  a constant [28]. It is important to note that transport losses are included in the scintillation process and that such effects end up being incorporated in the proposed thermal quenching analysis. These results are shown in Figure 7 as a continuous red line and yielded a thermal quenching activation energy of 0.38 eV.

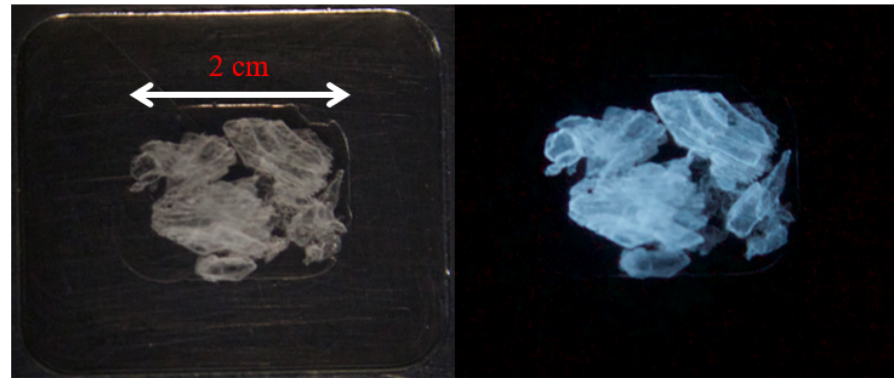


**Figure 5.** Optical images of  $\text{Rb}_4\text{Ge}_5\text{O}_9\text{F}_6:\text{Nb}$  crystals in the absence of X-rays (left) and of the same crystals scintillating under X-ray excitation (right).

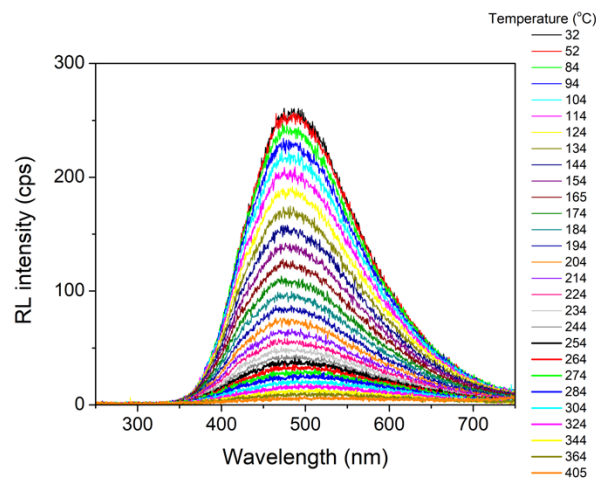


**Figure 6.** Selected RL spectra for  $\text{Rb}_4\text{Ge}_5\text{O}_9\text{F}_6:\text{Nb}$  up to 405 °C.

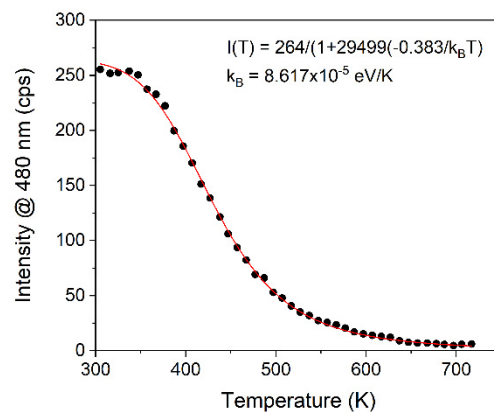


**Figure 7.** RL peak intensity at high temperatures (solid circles) together with fitting based on the Mott-Seitz model (red line).

### 3.3. EXAFS

The low Nb concentration within crystals of  $\text{Rb}_4\text{Ge}_5\text{O}_9\text{F}_6$ , <1% as determined by ICP-OES, contributed to a small amount of extra electron density relative to the undoped structure. Consequently, the location of Nb was not determinable using single-crystal X-ray diffraction data. To investigate the Nb local coordination environment, EXAFS measurements were performed. The results of the Nb K-edge experiments suggest Nb to be located in a six-fold coordination environment with bond lengths of approximately 2.0 Å. The approach included fitting the EXAFS signal for the known crystalline material,  $\text{Cs}_5\text{Nb}_3\text{O}_3\text{F}_{14}$ , which had a large edge jump and clear EXAFS signal from the absorption edge near 19 keV out to 19.8 keV, providing EXAFS data out to approximately  $15 \text{ \AA}^{-1}$ . The Nb ions in  $\text{Cs}_5\text{Nb}_3\text{O}_3\text{F}_{14}$  formed pairs of corner-shared  $\text{NbOF}_5$  octahedra and, although different from the coordination environment of Ge in  $\text{Rb}_4\text{Ge}_5\text{O}_9\text{F}_6$ , ( $\text{GeO}_3\text{F}_3$ ), which is expected to be occupied by Nb,  $\text{Cs}_5\text{Nb}_3\text{O}_3\text{F}_{14}$  provides a reliable standard for evaluating the data fitting approach. The results of measurements in fluorescence mode were fitted to the known structural model by refining only the amplitude reduction factor and the Debye-Waller factor for the first coordination sphere; see Figure 8. Figure 9 demonstrates that the single crystal model fits the EXAFS data well. The first shell bond lengths include one short Nb-O bond near 1.7 Å and 5 Nb-F bonds ranging from 1.9 to 2.2 Å.

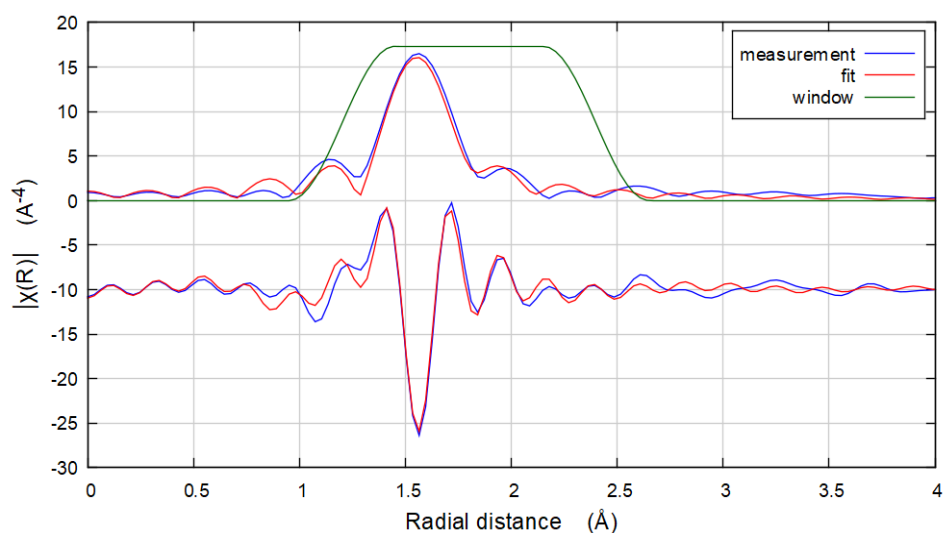


**Figure 8.** EXAFS fit (magnitude (top) and real part (bottom)) to the  $\text{Cs}_5\text{Nb}_3\text{O}_3\text{F}_{14}$  specimen using the single crystal model. Real space data were not plotted with phase shift correction, so bond lengths appear shorter than reported. Fitting parameters include: amplitude reduction factor = 0.83(7) and energy zero =  $-0.2(9)$  eV using three paths for the nearest neighbor oxygen and two nearest neighbor fluorine ions with Debye-Waller factors fixed at values of 0.001 Å<sup>2</sup>. Refinement R factor = 0.03 with reduced chi-squared of 2529.

The EXAFS spectrum for  $\text{Rb}_4\text{Ge}_5\text{O}_9\text{F}_6:\text{Nb}$  was of lower intensity, Figure 9, with a small absorption edge step, rendering the amplitudes unreliable for direct determination of the coordination number. However, the bond lengths can be easily extracted from these results using a single-path fit. The parent structure has three distinct Ge sites, two of which are tetrahedral with 1.74 and 1.75 Å average Ge-O bond lengths and one of which is octahedral with an average Ge-O bond length of 1.84 Å.  $\text{Nb}^{5+}$  replacing a Ge ion leads to three possible Nb configurations: all octahedral, all tetrahedral, or a mix of both. The model yields an average Nb first coordination shell at 2.03(4) Å, suggesting that the coordination is 6-fold. A related oxide structure with similar polyhedral linkages,  $\text{Cs}_2\text{Nb}_4\text{O}_{11}$ , has average Nb-O distances of 1.85 Å in tetrahedral coordination and 1.97 Å in octahedral coordination [29]. The EXAFS data suggest octahedral coordination for the niobium given that the bond lengths derived from the EXAFS data are close to those found for octahedral Ge-F and

Ge-O bond lengths and, in fact, slightly longer, which is consistent with the fact that they represent Nb-F and Nb-O bonds.

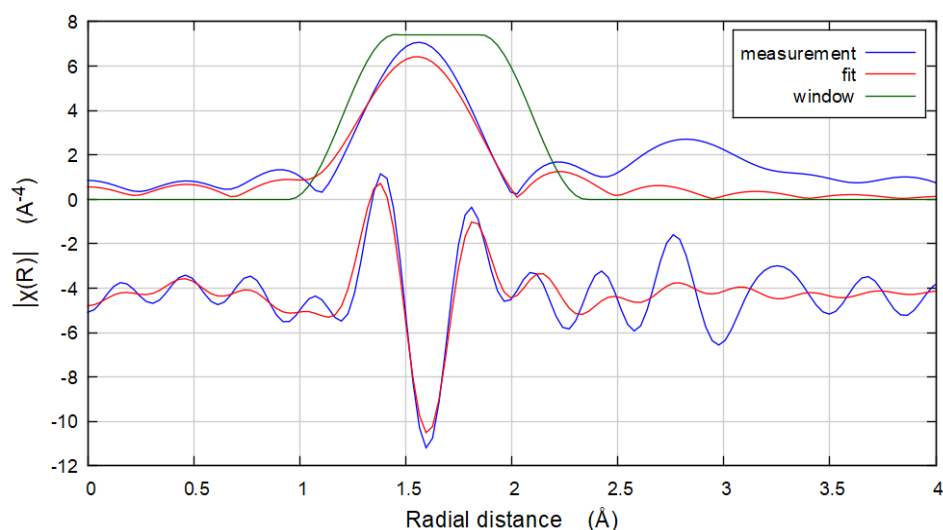


**Figure 9.** EXAFS fit (magnitude (top) and real part (bottom)) to the  $\text{Rb}_4\text{Ge}_5\text{O}_9\text{F}_6:\text{Nb}$  specimen with focus on determining first shell bond lengths. Real space data were not plotted with phase shift correction, so bond lengths appear shorter than reported. The refined values indicate the first shell average bond length, fit using one path, is  $2.03(4)$  Å. The refined Debye-Waller factor is  $0.003(2)\text{Å}^2$ , with a refinement R factor of 0.03 with reduced chi-squared of 3459.

#### 4. Conclusions

In summary, a new inorganic scintillating material,  $\text{Rb}_4\text{Ge}_5\text{O}_9\text{F}_6:\text{Nb}$ , was discovered and prepared in single crystal form through niobium doping using a high-temperature  $\text{RbCl}/\text{RbF}$  flux. The crystal structure consists of layers containing  $\text{GeO}_3\text{F}_3$  octahedra connected by cyclic  $\text{Ge}_3\text{O}_9$  units, with the layers separated by Rb atoms. The crystals emit bright blue light under UV light exposure and, additionally, emit blue light under X-ray radiation. The observed fluorescence is caused by a small percentage of Nb incorporated into the structure that likely occupies an octahedral coordination environment, as suggested by EXAFS experiments.

**Supplementary Materials:** The following supporting information can be downloaded at: <https://www.mdpi.com/article/10.3390/inorganics10060083/s1>. Figure S1: Powder X-ray diffraction pattern for  $\text{Rb}_4\text{Ge}_5\text{O}_9\text{F}_6:\text{Nb}$ .

**Author Contributions:** Formal analysis, D.C., V.V.K., S.T.M., J.C.S., L.G.J., M.A., J.S.-P. and S.A.J.T.; investigation, D.C., V.V.K. and A.T.H.; writing—original draft preparation, D.C. and V.V.K.; writing—review and editing, H.-C.z.L.; supervision, T.M.B. and H.-C.z.L. All authors have read and agreed to the published version of the manuscript.

**Funding:** Financial support for this work was provided by the National Science Foundation under DMR 1806279, which supported the synthesis, structural characterization, and optical measurements, and DMR-1653016, which supported the radioluminescence measurements. Beam time for the X-ray absorption spectroscopy study was provided by MRCAT. MRCAT operations are supported by the Department of Energy and the MRCAT member institutions. This research used resources of the Advanced Photon Source, a U.S. Department of Energy (DOE) Office of Science User Facility operated for the DOE Office of Science by Argonne National Laboratory under Contract No. DE-AC02-06CH11357.

**Data Availability Statement:** CCDC 2039182 and 2170938 contain the supplementary crystallographic data for this paper. This data can be obtained free of charge via [www.ccdc.cam.ac.uk/data\\_request/cif](http://www.ccdc.cam.ac.uk/data_request/cif), or by emailing [data\\_request@ccdc.cam.ac.uk](mailto:data_request@ccdc.cam.ac.uk), or by contacting The Cambridge Crystallographic Data Centre, 12 Union Road, Cambridge CB2 1EZ, UK; fax: +44-1223-336033.

**Conflicts of Interest:** The authors declare no conflict of interest.

## References

1. Yoshida, E.; Hirano, Y.; Tashima, H.; Inadama, N.; Nishikido, F.; Moriya, T.; Omura, T.; Watanabe, M.; Murayama, H.; Yamaya, T. The X'tal cube PET detector with a monolithic crystal processed by the 3D sub-surface laser engraving technique: Performance comparison with glued crystal elements. *Nucl. Instrum. Methods Phys. Res. Sect. A* **2013**, *723*, 83–88. [[CrossRef](#)]
2. Tous, J.; Blazek, K.; Pina, L.; Sopko, B. High-resolution imaging of biological and other objects with an X-ray digital camera. *Appl. Radiat. Isot.* **2010**, *68*, 651–653. [[CrossRef](#)] [[PubMed](#)]
3. Danevich, F.A.; Chernyak, D.M.; Dubovik, A.M.; Grinyov, B.V.; Henry, S.; Kraus, H.; Kudovbenko, V.M.; Mikhailik, V.B.; Nagornaya, L.L.; Podviyanuk, R.B.; et al. MgWO<sub>4</sub>-A new crystal scintillator. *Nucl. Instrum. Methods Phys. Res. Sect. A* **2009**, *608*, 107–115. [[CrossRef](#)]
4. Carone, D.; Jacobsohn, L.G.; Breton, L.S.; zur Loye, H.-C. Synthesis, structure, and scintillation of Rb<sub>4</sub>Ta<sub>2</sub>Si<sub>8</sub>O<sub>23</sub>. *Solid State Sci.* **2022**, *127*, 106861. [[CrossRef](#)]
5. Juillerat, C.A.; Kocevski, V.; Morrison, G.; Karakalos, S.G.; Patil, D.; Mixture, S.T.; Besmann, T.M.; zur Loye, H.-C. Flux crystal growth of uranium(v) containing oxyfluoride perovskites. *Inorg. Chem. Front.* **2019**, *6*, 3203–3214. [[CrossRef](#)]
6. Morrison, G.; zur Loye, H.-C. Flux Growth of [NaK<sub>6</sub>F][(UO<sub>2</sub>)<sub>3</sub>(Si<sub>2</sub>O<sub>7</sub>)<sub>2</sub>] and [KK<sub>6</sub>Cl][(UO<sub>2</sub>)<sub>3</sub>(Si<sub>2</sub>O<sub>7</sub>)<sub>2</sub>]: The Effect of Surface Area to Volume Ratios on Reaction Products. *Cryst. Growth Des.* **2016**, *16*, 1294–1299. [[CrossRef](#)]
7. Morrison, G.; Tran, T.T.; Halasyamani, P.S.; zur Loye, H.-C. K<sub>8</sub>(K<sub>5</sub>F)U<sub>6</sub>Si<sub>8</sub>O<sub>40</sub>: An Intergrowth Uranyl Silicate. *Inorg. Chem.* **2016**, *55*, 3215–3217. [[CrossRef](#)]
8. Morrison, G.; Smith, M.D.; zur Loye, H.-C. Understanding the Formation of Salt-Inclusion Phases: An Enhanced Flux Growth Method for the Targeted Synthesis of Salt-Inclusion Cesium Halide Uranyl Silicates. *J. Am. Chem. Soc.* **2016**, *138*, 7121–7129. [[CrossRef](#)]
9. Spagnuolo, N.R.; Morrison, G.; zur Loye, H.-C. Synthesis and crystal structure of [(Cs<sub>6</sub>F)(Cs<sub>3</sub>AgF)][Ge<sub>14</sub>O<sub>32</sub>] through alkali halide flux growth. *Solid State Sci.* **2019**, *97*, 105973. [[CrossRef](#)]
10. Latshaw, A.M.; Wilkins, B.O.; Hughey, K.D.; Yeon, J.; Williams, D.E.; Tran, T.T.; Halasyamani, P.S.; zur Loye, H.-C. A<sub>5</sub>RE<sub>4</sub>X[TO<sub>4</sub>]<sub>4</sub> crystal growth and photoluminescence. Fluoride flux synthesis of sodium and potassium rare earth silicate oxyfluorides. *CrystEngComm* **2015**, *17*, 4654–4661. [[CrossRef](#)]
11. Latshaw, A.M.; Morrison, G.; zur Loye, H.-C.; Myers, A.R.; Smith, M.D.; zur Loye, H.-C. Intrinsic blue-white luminescence, luminescence color tunability, synthesis, structure, and polymorphism of K<sub>3</sub>YSi<sub>2</sub>O<sub>7</sub>. *CrystEngComm* **2016**, *18*, 2294–2302. [[CrossRef](#)]
12. Morrison, G.; Latshaw, A.M.; Spagnuolo, N.R.; zur Loye, H.-C. Observation of Intense X-ray Scintillation in a Family of Mixed Anion Silicates, Cs<sub>3</sub>RESi<sub>4</sub>O<sub>10</sub>F<sub>2</sub> (RE = Y, Eu–Lu), Obtained via an Enhanced Flux Crystal Growth Technique. *J. Am. Chem. Soc.* **2017**, *139*, 14743–14748. [[CrossRef](#)]
13. Ayer, G.B.; Klepov, V.V.; Smith, M.D.; Hu, M.; Yang, Z.; Martin, C.R.; Morrison, G.; zur Loye, H.-C. BaWO<sub>2</sub>F<sub>4</sub>: A mixed anion X-ray scintillator with excellent photoluminescence quantum efficiency. *Dalton Trans.* **2020**, *49*, 10734–10739. [[CrossRef](#)] [[PubMed](#)]
14. Hizhnyi, Y.; Nedilko, S.G.; Chornii, V.P.; Nikolaenko, T.M.; Slobodyanik, N.S.; Sheludko, V.I. Structure of the fluorine states in cadmium molybdate host studied by the electronic band structure calculations of CdMoO<sub>4</sub>, CdMoO<sub>4</sub>:F and CdMoO<sub>3</sub>F<sub>2</sub> crystals. *Comput. Mater. Sci.* **2014**, *87*, 12–18. [[CrossRef](#)]
15. Kozlov, A.V.; Pustovarov, V.A.; Sarychev, M.N.; Isaenko, L.I. Luminescence Spectroscopy of Rb<sub>2</sub>KTiOF<sub>5</sub> Oxyfluoride Single Crystals. *AIP Conf. Proc.* **2017**, *1886*, 020012.
16. Srivastava, A.M.; Ackerman, J.F. Synthesis and luminescence properties of Cs<sub>2</sub>NbOF<sub>5</sub> and Cs<sub>2</sub>NbOCl<sub>5</sub> with isolated [NbOX<sub>5</sub>]<sup>2-</sup> (X = F, Cl) octahedra. *Mater. Res. Bull.* **1991**, *26*, 443–448. [[CrossRef](#)]
17. Krause, L.; Herbst-Irmer, R.; Sheldrick, G.M.; Stalke, D. Comparison of Silver and Molybdenum Microfocus X-ray sources for Single-Crystal Structure Determination. *J. Appl. Crystallogr.* **2015**, *48*, 3–10. [[CrossRef](#)]
18. Bruker. APEX3, SAINT+, TWINABS, and SADABS; Bruker AXS Inc.: Madison, WI, USA, 2015.
19. Dolomanov, O.V.; Bourhis, L.J.; Gildea, R.J.; Howard, J.A.; Puschmann, H. OLEX2: A Complete Structure Solution, Refinement and Analysis Program. *J. Appl. Crystallogr.* **2009**, *42*, 334–341. [[CrossRef](#)]
20. Sheldrick, G.M. Crystal Structure Refinement with SHELXL. *Acta Crystallogr. Sect. C Struct. Chem.* **2015**, *71*, 3–8. [[CrossRef](#)]
21. Spek, A.L. Structure Validation in Chemical Crystallography. *Acta Crystallogr. Sect. D Biol. Crystallogr.* **2009**, *65*, 148–155. [[CrossRef](#)]
22. Ravel, B.; Newville, M. ATHENA, ARTEMIS, HEPHAESTUS: Data analysis for X-ray absorption spectroscopy using IFEFFIT. *J. Synchrotron. Radiat.* **2005**, *12*, 537–541. [[CrossRef](#)] [[PubMed](#)]
23. Conradsson, T.; Zou, X.; Dadachov, M.S. Synthesis and Crystal Structure of a Novel Germanate: (NH<sub>4</sub>)<sub>4</sub>[(GeO<sub>2</sub>)<sub>3</sub>(GeO<sub>1.5</sub>F<sub>3</sub>)<sub>2</sub>]-0.67H<sub>2</sub>O. *Inorg. Chem.* **2000**, *39*, 1716–1720. [[CrossRef](#)] [[PubMed](#)]
24. Aluker, E.D. Temperature dependence of scintillation response in NaI(Tl), KI(Tl), CsI(Tl). *Phys Lett.* **1965**, *14*, 17–18. [[CrossRef](#)]

25. Aluker, E.D.; Mezina, I.P. The temperature dependence of radioluminescence yield in alkali halide crystal phosphors. *Phys. Stat. Sol.* **1967**, *19*, 35–40. [[CrossRef](#)]
26. Wu, Y.; Meng, F.; Li, Q.; Koschan, M.; Melcher, C.L. Role of Ce<sup>4+</sup> in the scintillation mechanism of codoped Gd<sub>3</sub>Ga<sub>3</sub>Al<sub>2</sub>O<sub>12</sub>:Ce. *Phys. Rev. Appl.* **2014**, *2*, 044009. [[CrossRef](#)]
27. Trofimov, A.A.; Jacobsohn, L.G. Radioluminescence of Lu<sub>3</sub>Al<sub>5</sub>O<sub>12</sub>:Ce single crystal and transparent polycrystalline ceramic at high temperatures. *Ceram. Int.* **2020**, *46*, 26335–26338. [[CrossRef](#)]
28. Botter-Jensen, L.; McKeever, S.W.S.; Wintle, A.G. *Optically Stimulated Luminescence Dosimetry*; Elsevier: Amsterdam, The Netherlands, 2003.
29. Smith, R.W.; Hu, C.; Liu, J.; Mei, W.-N.; Lin, K.-J. Structure and antiferroelectric properties of cesium niobate, Cs<sub>2</sub>Nb<sub>4</sub>O<sub>11</sub>. *J. Solid State Chem.* **2007**, *180*, 1193–1197. [[CrossRef](#)]